Journal of Maps

ISSN: (Print) (Online) Journal homepage: https://www.tandfonline.com/loi/tjom20

Indoor radon measurements in Calabria (Southern Italy)

Valeria Lupiano, Salvatore Procopio, Gabriele Buttafuoco, Valeria Rago & Giulio Iovine

To cite this article: Valeria Lupiano, Salvatore Procopio, Gabriele Buttafuoco, Valeria Rago & Giulio Iovine (2023) Indoor radon measurements in Calabria (Southern Italy), Journal of Maps, 19:1, 2132883, DOI: 10.1080/17445647.2022.2132883

To link to this article: https://doi.org/10.1080/17445647.2022.2132883

JOURNAL OF MAPS
2023, VOL. 19, NO. 1, 2132883
https://doi.org/10.1080/17445647.2022.2132883

SCIENCE

OPEN ACCESS Check for updates

Indoor radon measurements in Calabria (Southern Italy)

Valeria Lupiano [a], Salvatore Procopio[b], Gabriele Buttafuoco [c], Valeria Rago [a] and Giulio Iovine [a]

[a]National Research Council of Italy, Research Institute for Geo-Hydrological Protection, CNR-IRPI, Cosenza, Italy; [b]Regional Agency for the Protection of the Calabrian Environment, ARPACal, Catanzaro, Italy; [c]National Research Council of Italy, Institute for Agricultural and Forest Systems in the Mediterranean, Rende, Italy

ABSTRACT

Radon gas from the ground is the main source of indoor concentrations in buildings, regardless of construction characteristics. According to Council Directive 2013/59/EURATOM, EU Member States must establish national reference levels for indoor radon concentrations in workplaces and draw up a National Radon Plan. In Calabria (Southern Italy), maps of indoor measurements at regional scale are not available. A set of 1434 average annual measurements, taken between 2010 and 2021, has been analysed. For a limited sector, a geostatistical approach allowed to map the expected concentrations at ground floor, the spatial uncertainty of estimates, and the probability of exceedance of the 300 Bq m^{-3} Italian threshold for workplaces. Highest values characterize the eastern border of the Sila massif. Obtained maps might be used to optimize locations of additional dosimeters, based on geological constraints. Such studies may support urban planning policies and provide recommendations on building techniques.

ARTICLE HISTORY
Received 14 December 2021
Revised 27 September 2022
Accepted 27 September 2022

KEYWORDS
Radon gas; indoor measurement; geostatistics; Calabria

1. Introduction

The main natural source of radiation for humans is radon gas from the ground, with critical exposures mostly related to inflow into buildings (Cinelli et al., 2019; Zeeb et al., 2009). In addition to geological factors, indoor concentrations depend on construction methods and types of use of the buildings. Inhalation and ingestion of radon decay products is the second major cause of lung cancer (after smoking), and the primary cause for non-smokers (Ielsch et al., 2001; Nazaroff, 1992; Steinbuch et al., 1999; Vienneau et al., 2021; Zeeb et al., 2009). The largest doses of radiation come from Radon-222, a colourless, odourless and almost chemically inert radioactive gas. Radon-222 is the radioactive decay product of Radium-226, one of the terms of the natural decay of Uranium. Radium-226 is ubiquitous in rocks and soils, with concentrations depending on mineralogy (Choubey et al., 1999; Choubey & Ramola, 1997; Choubey et al., 1997; Clamp & Pritchard, 1998; Gundersen, 1992; Gundersen et al., 1992; Minda et al., 2009; Tanner, 1964). Despite its short half-life (3.82 days), Radon-222 can escape from the soil before decaying into a series of short-lived radioactive progeny, with the emission of alpha particles (Darby et al., 2005).

Previous studies in Italy were mainly focused on geogenic radon gas in the soil to identify 'prone areas' (e.g. Giustini et al., 2019; Iovine et al., 2018). Geogenic potential maps were developed by employing geostatistical approaches. Particularly, in Calabria (southern Italy), studies were only performed in northern and central areas (Buttafuoco et al., 2007; Iovine et al., 2018; Tansi et al., 2005). More in detail, Tansi et al. (2005) found no evidence of a strong correlation between lithology and radon concentrations in the south-eastern portion of the Crati graben (northern Calabria). Instead, a clear correlation between the elongated shape of anomalies and the orientation of the main N–S trending faults could be recognized – except for the southernmost sector, where concentrations are affected by the superposition of the same structures with those belonging to another regional fault system, trending NW–SE. Higher concentrations were also observed in the epicentral zones of instrumental or historical earthquakes, whereas lower values were found in areas affected by large-scale landslides. Buttafuoco et al. (2007) explored the spatial structure of radon concentrations in the northern part of the Crati graben by a geostatistical analysis and compared the prediction performances of four different algorithms. Buttafuoco et al. (2010) investigated the relationships between radon concentrations, geology and structural patterns in the Catanzaro-Lamezia plain (central Calabria) and assessed the spatial uncertainty associated with the prediction of geogenic radon in the soil through

CONTACT Valeria Rago ragovaleria@gmail.com
Supplemental map for this article can be accessed at https://doi.org/10.1080/17445647.2022.2132883.

conditional sequential Gaussian simulation (Chilès & Delfiner, 2012). Emanation resulted to be somehow affected by faults, lithology and basement geochemistry. More recently, Iovine et al. (2018) made a schematic review of worldwide data on soil-gas radon amounts versus geological factors. Concentrations surveyed in three Calabrian study areas were also analysed against lithotypes and faults, by considering spatial variations. No appreciable differences in concentrations could be ascribed to lithotypes, whereas a clear relation with the main faults was recognized.

Zeeb et al. (2009) recommended reference values between 100 and 300 Bq m^{-3} for indoor radon concentrations. The Council Directive 2013/59/EURATOM on 'basic safety standards' for protection against exposure to ionizing radiations was implemented in the Italian Legislative Decree n. 101/2020, in September 2020. The above Directive applies to the exposure of workers or public to indoor radon, besides external exposure from building materials, and long-term exposure from emergencies and human activity. In accordance, EU Member States must establish national thresholds for indoor radon concentrations in workplaces. In Italy, for annual average activity concentration in air, such levels should not generally exceed the threshold of 300 Bq m^{-3} (*note*: starting from December 2024, the threshold will be reduced to 200 Bq m^{-3} for new buildings).

Addressing radon is an important task for risk prevention in new buildings, and for mitigation/remediation purposes in existing buildings (Zeeb et al., 2009). Indoor measurements of concentration are relatively simple to carry out (Ciolini & Mazed, 2010), and generally point out a strong relationship with building characteristics, besides geological factors (e.g. Cafaro et al., 2014; Giustini et al., 2019; Sabbarese et al., 2021). In such studies, indoor radon concentrations were generally found to be affected by clustering and apparent non-stationarity issues.

In literature, maps of indoor radon at regional scale are not available for Calabria. The Joint Research Centre of the European Commission published the digital version (Cinelli et al., 2019) of the *European Atlas of natural radiation* (De Cort et al., 2011) that includes a map of indoor radon concentration in ground floor rooms of dwellings in Europe – in which great part of southern Italy is not covered. Furthermore, modelling uncertainty is often disregarded – particularly, the spatial uncertainty that arises from the fact that even if the data are perfectly measured, they are sparse and nothing is known at unmeasured locations (Caers, 2011; Heuvelink, 2018).

In this study, indoor radon measurements, taken by the Regional Agency for Environmental Protection in Calabria (ARPACal) are analysed and mapped. The inherent high variability of measurements made it possible to assess the feasibility of pattern recognition, trend and classification approaches of indoor data. In the Main map, measurements are shown on a lithostructural map at 1:250,000 scale. The same measurements are also shown on smaller-scale maps (1:1,000,000), based on the floor (Figure A: higher floors, Figure B: first floor, Figure C: ground floor, Figure D: basement). In Annex A, the list of surveyed villages with main statistics is reported. In Annex B, measurements with administrative and territorial details are listed. Figure E shows the results of modelling the spatial distribution of measurements at ground floor by a geostatistical approach.

2. Geological setting

In Calabria (Figure 1 and 2), crystalline-metamorphic nappes (Palaeozoic), thrust onto the Mesozoic-Cenozoic units of the Apennine chain, are diffusely covered by sedimentary rocks (Miocene-Quaternary). Ophiolite-bearing tectonic units (Jurassic to Early Cretaceous), overlying basement nappes, Hercynian and pre-Hercynian in age, crop out (Amodio-Morelli et al., 1976; Tortorici et al., 1995). Since Middle Miocene, overthrusting and migration of the Arc towards southeast along a regional NW–SE fault system combined with the opening of the Tyrrhenian basin (Van Dijk et al., 2000). Between Late Pliocene and Early Quaternary, the Arc was dissected by longitudinal and transversal normal faults (Tansi et al., 2007). From Middle Pleistocene, a WNW-ESE extensional phase resulted in the 'Calabrian-Sicilian rift-zone', an active normal fault belt along the western coast (Monaco & Tortorici, 2000). Due to such a complex geodynamic history, rocks generally show high-grade weathering.

3. Materials and methods

Radon protection is included in the mission of ARPACal and is mainly carried out by monitoring indoor concentrations and maintaining a database of measurements. Between 2010 and 2021, long-term measurements of indoor radon concentration were carried out by time-integrated passive dosimeters, containing CR-39 Solid State Nuclear Track Detector (SSNTD) (Fonseca, 1983; Bing, 1993). The physical test for determining the concentration of indoor radon gas activity, according to the quality system accreditation of the ARPACal Laboratory (Accredia Lab n. 1616L), has a precision of 4% and an accuracy of 9% in the exposure range 60–6000 kBq m^{-3} h.

Dosimeters were located according to a randomized design and collected at each site twice a year, allowing to compute annual averages. The choice of the floor in which the measurements had to be made depending on the building type (*S – school*, *W – workplace*, *D – dwelling* – all of them built in reinforced

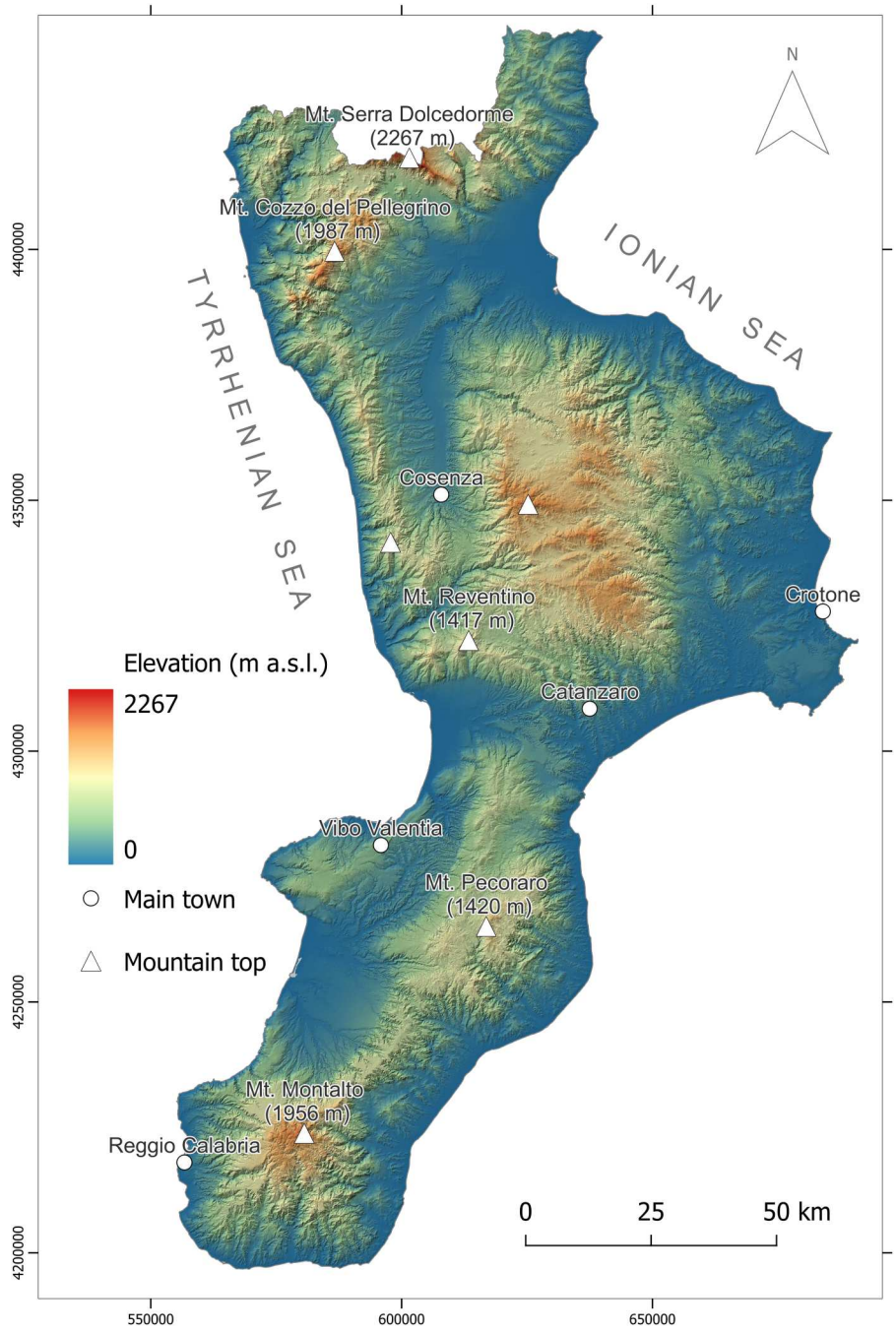

Figure 1. Elevation map of Calabria, with indication of the main towns and toponyms.

concrete), as well as on agreements with the owners and on privacy/legal constraints.

In the database, each measurement is listed by an identification code (ID); location (coordinates), address, and floor; dosimeter type; start and end of measurement. Indoor data underwent preliminary quality control to ensure reliability. Different types of potential 'noise' (e.g. measurement errors, typos, wrong coordinates) were checked, even to recognise true outliers in the statistical distribution. Coordinates were verified also by check the crossing addresses with apparent positions. The positional accuracy of the locations taken by GPS devices is about 3–4 m (in residential complexes made of several buildings, operators took only a single position for a set of nearby measurement locations). Data were georeferenced in the coordinate system UTM WGS84 33N (EPSG code: 32633) and imported into a GIS as *points vector* format.

Lithotypes shown in the Main map were derived from the Geological Map of Calabria in scale 1:25,000 (CASMEZ, 1969), based on the expected similarity of radon concentrations (Iovine et al., 2018). Outcropping terrains were grouped into 8 classes, as follows: (a) *cS – coarse-grained sediment*; (b) *fS – fine-grained sediment*; (c) *LE – limestone and evaporite*; (d) *F – flysch*; (e) *lM – low-grade metamorphic rock*; (f) *mhM – medium/high-grade metamorphic rock*; (g) *aMa – acid magmatic rock*; (h) *bMa – basic magmatic rock*.

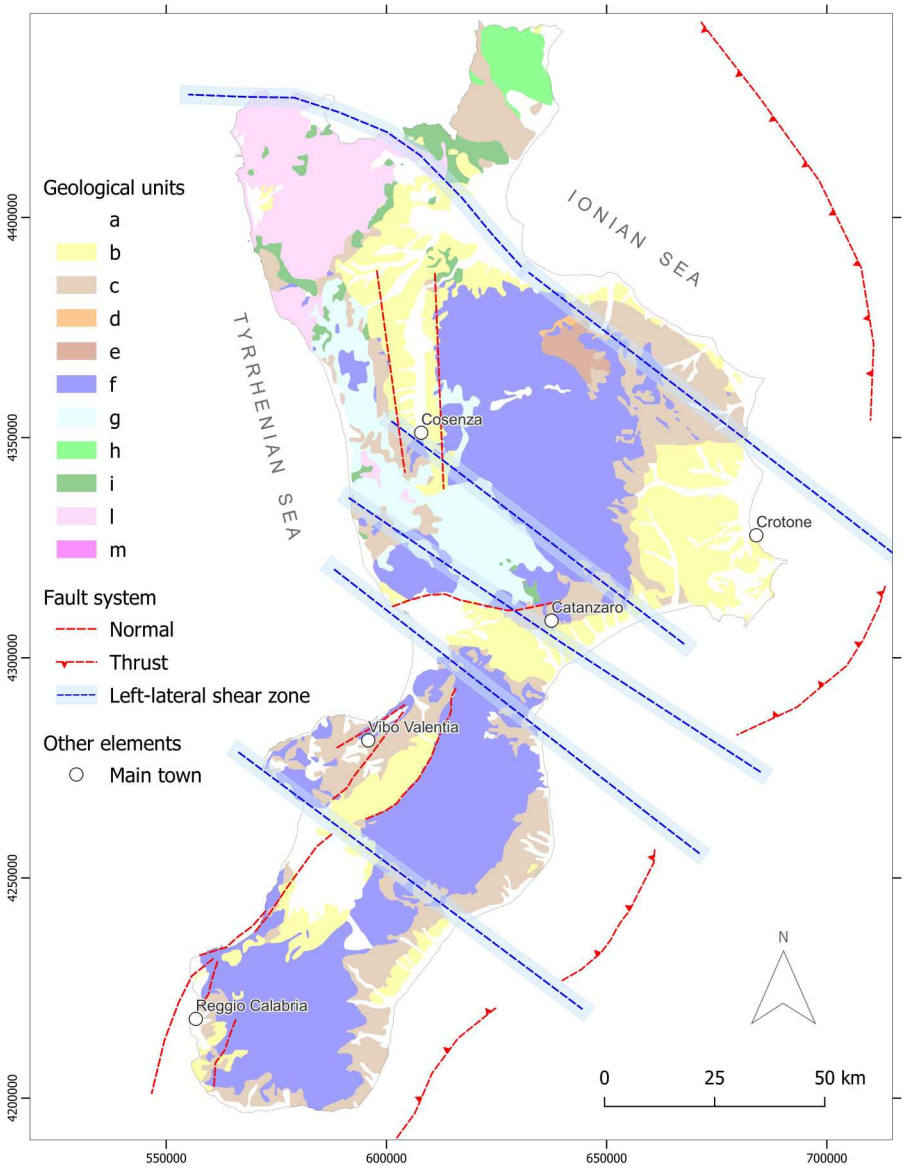

Figure 2. Geological scheme (after Vitale, Ciarcia, Fedele, & Tramparulo, 2019, mod.), with main fault systems (after Monaco & Tortorici, 2000; Van Dijk et al., 2000; Tansi et al., 2007; mod.). Key: *Unconformable Deposits* – (a) Quaternary deposit; (b) Pliocene deposit; (c) Miocene deposit; (d) Paludi Fm. (Late Oligocene-Aquitanian); *Calabria-Peloritani Terrane (overriding plate)* – (e) Eocene cover (Longobucco F.); (f) not affected by Alpine metamorphism (Sila and Stilo units, Palaeozoic-Eocene); (g) affected by Alpine metamorphism (Bagni, Castagna, Aspromonte, Africo-Polsi, Peloritani Mts. units, Palaeozoic-Cretaceous); *Southern Ligurian Domain (oceanic suture), obducted units* – (h) Ligurian Accretionary Complex, Nord-Calabrese, Parasicilide and Sicilide units (Late Cretaceous–early Miocene); *subducted units* – (i) Frido, Diamante-Terranova, Malvito and Gimigliano units (Jurassic-Late Oligocene); Adria Domain *(downgoing plate), Apennine Carbonate Platform units* – (l) metamorphic units (Lungro-Verbicaro and Cetraro units, Middle Triassic-early Miocene); (m) Lagonegro-Molise Basin units (Triassic-Miocene).

The main geological structures in the Main map were derived from the ITHACA (2021) Catalogue and from the above-mentioned Geological Map of Calabria. In particular, 'active and capable' faults were extracted from ITHACA and shown as *recent faults*. Note that, according to the above Catalogue, such tectonic structures are considered 'active' as they moved in the recent geologic past (i.e. between Upper Pleistocene to Present) and are expected to move again within a future time span of concern for the safety of a nuclear installation. Moreover, they are defined 'capable' as they have a significant potential for displacement at or near the ground surface. Based on available information on kinematics, such structures could further be distinguished into two classes as follows: normal, and oblique/strike slip. Older tectonic structures were extracted from the CASMEZ geological maps and shown as *ancient faults* (undefined kinematics).

The contour lines (equidistance at 500 m) shown in the Main map and the shaded relief in the A-E maps were obtained from the digital elevation model TINITALY (Tarquini et al., 2007), a grid of square cells with a side of 10 m.

Indoor radon concentration measurements were analysed with respect to the 8 lithological classes for

the whole sample (1434 values), either in the vicinity ('inside buffer', 145 values) or far from faults ('outside buffer', 1289 values). Buffers were built with different widths, according to the level of mapping accuracy (300 and 150 m for uncertain and certain faults, resp.).

By selecting only measurements taken at the ground floor, the mean indoor concentrations and their upper and lower limits (at the 95% confidence level) were computed to verify any control by lithology. To this purpose, indoor concentrations were first transformed into Gaussian values by means of a *Gaussian anamorphosis* (Chilès & Delfiner, 2012), and then back transformed into raw values.

Aimed at investigating the properties of the spatial structure of indoor radon concentrations, and of their spatial distribution, a '*sector of interest*' was then delimited by drawing a polygon including most of the measurement locations. Only the measurements taken at the ground floor (subsample = 940 measurements, 86 thereof inside and 854 outside the fault buffers) were used in the geostatistical analysis (i.e. the most numerous subsample).

Indoor data were modelled as an intrinsic, stationary process: each datum $z(\mathbf{x}_\alpha)$ – where $\mathbf{x}$ is the location coordinates vector, and α the sampling point $1, \ldots, N$ – was interpreted as a particular realization (outcome) of a random, regionalized variable $Z(\mathbf{x}_\alpha)$. At unsampled locations, values $z(\mathbf{x}_\alpha)$ are unknown but also well-defined because they can be considered as outcomes of the corresponding random variable $Z(x_\alpha)$ (Armstrong, 1998). The set of spatially dependent random variables forms a random function. For more details, see – among others – Goovaerts (1997), Chilès and Delfiner (2012), Wackernagel (2003), Webster and Oliver (2007).

An experimental variogram was calculated for structural data interpretation, and a theoretical model of variogram was fitted for spatial interpolation (Chilès & Delfiner, 2012; Matheron, 1971). Ordinary kriging (OK) is one of the most basic types of kriging methods: it only uses primary information and provides an error variance (Webster & Oliver, 2007). Nevertheless, OK produces a smoothing effect and, to better visualize heterogeneity and assess the uncertainty of concentrations at unsampled locations, single estimates can be replaced by stochastic simulations, thus producing a set of alternative maps (possible 'realities' or 'realizations') of Rn concentrations that honour sample information and also attempt to reproduce their spatial variability (Chilès & Delfiner, 2012). Among the stochastic simulation techniques, the '*turning bands method*' (Matheron, 1973) – a simulation technique that requires a multi-Gaussian framework – was used, and a number of 500 realizations were established. Accordingly, indoor data were transformed into a normal-distribution-shaped variable, with zero mean and unit variance, by using the *Gaussian anamorphosis* (Chilès & Delfiner, 2012). The measured radon concentrations were used as conditioning data, and the differences between the simulated maps convey the uncertainty about true concentrations. The pixel-by-pixel histograms summarize the different simulations and approximate the probability distribution functions that correspond to each node of the grid. By averaging the simulated values for each pixel (Journel, 1983), maps of '*expected*' values at any location and the related standard deviations could be obtained. The standard deviation provides a measure of uncertainty on the 'true value' of radon concentration. Finally, by counting the stochastic images exceeding a given threshold, and converting the sum to a proportion, the probability of exceeding a given threshold could be computed. In this study, a value of 300 Bq m^{-3} for annual average activity concentration in air was considered to map the empirical probability of exceedance of the Italian legal threshold for workplaces.

4. Results and discussion

The total set of 1434 indoor radon measurements is shown on the litho-structural map at 1:250,000 scale (Main map). The same measurements are included in 1:1,000,000 scale maps, separately by floors (Figure A: higher floors, Figure B: first floor, Figure C: ground floor, Figure D: basement). In all the maps, concentrations are shown by classes, delimited by also considering the mentioned reference thresholds for indoor radon gas (100, 200 and 300 Bq m^{-3}).

As a whole, measurements were carried out in 133 (out of 404) different municipalities, unevenly distributed in the five Calabrian provinces (Table 1). The greatest number of measurements was performed in the Catanzaro province (ca. 46%), whereas only 6% in the Reggio Calabria one. The list of municipalities considered in the survey is listed by province in Annex A, with main statistics on the measurements. In Annex B, average concentrations are listed for all the measurement sites, with administrative and territorial details.

Most measurements were performed at the ground floor (ca. 71% – cf. Table 2). The minimum value obtained for indoor concentration is 6.77 Bq m^{-3}, whereas the maximum is 1934 Bq m^{-3}, both measured

Table 1. Number of measurements by province, for the whole sample (N) and for the ground floor subsample (N^0).

Province	N	$N > 300$ Bq m^{-3}	N^0	$N^0 > 300$ Bq m^{-3}
Cosenza	200	24	150	17
Catanzaro	**662**	**41**	**434**	24
Crotone	227	33	160	**27**
Reggio di Calabria	*92*	*4*	*63*	*4*
Vibo Valentia	253	17	216	10
Tot.	**1434**	**119**	**1023**	**82**

at ground floor in dwellings (Table 3). In particular, values above 900 Bq m^{-3} (i.e. 3 times the legal threshold) were obtained (Table 4): in five schools, two workplaces and two dwellings; mostly, in the Crotone province; within urbanized areas; at ground floor; on coarse-grained sediments; 5 km from the nearest active fault (but less than 1 km from a generic fault), in average. No clear correlations could be appreciated with respect to fault kinematics.

Table 5 summarizes the measurements performed by lithological classes, for the whole sample. Results are shown for the subsamples of measurements carried out inside (10%) or outside (90%) the fault buffers.

Similarly, statistics related to the 1023 measurements made at *ground floor* are reported in Tables 1, 6 and 7. For this subsample, values above 900 Bq m^{-3} were only obtained in four schools, two dwellings and one workplace. Table 7 summarize the number of measurements distributed by lithological classes, obtained either in the vicinity (inside buffer) or far from geological structures (outside buffer).

Note that, in all the tables, maxima are listed in bold, and minima in italics; the number of measurements exceeding the threshold of 300 Bq m^{-3} are also listed.

In Figure 3, means of indoor concentrations (subsample: ground floor) and their intervals of confidence (upper and lower limits at the 95% confidence level) are shown, with reference to the eight lithological classes. Highest values are generally to be found on *bMa* and on *lM*, followed by *mhM* and *aMa*, for locations located either 'within' or 'outside' the fault buffers. Nevertheless, no strong differences can be appreciated in the mean values with respect to

Table 2. Number of measurements (*N*), and range of concentrations by floor, for the whole sample.

Floor	*N*	Minimum (Bq m^{-3})	Maximum (Bq m^{-3})	*N* > 300 Bq m^{-3}
Basement	143	19.06	1157.00	31
Ground	**1023**	*6.77*	**1934.00**	**82**
First	200	7.00	658.00	6
Second	50	14.91	151.00	*0*
Third	15	21.20	119.00	*0*
Fourth	*3*	**67.00**	*117.00*	*0*
Tot.	**1434**			**119**

Table 3. Number of measurements (*N*), and range of concentrations by type of use of the building, for the whole sample.

Type of use	*N*	Minimum (Bq m^{-3})	Maximum (Bq m^{-3})	*N* > 300 Bq m^{-3}
Dwelling	**653**	*6.77*	**1934.00**	**48**
School	409	**13.42**	*1209.37*	38
Workplace	*372*	12.00	1701.75	*33*
Tot.	**1434**			**119**

Table 4. Radon measurements exceeding 900 Bq m^{-3}.

ID	Elevation m a.s.l. (ground)	Province	Municipality	Floor	Type of building	Start of measure (date)	End of measure (date)	Concentration of activity (Bq m^{-3})	Uncertainty (Bq m^{-3})	Lithotype	Distance from nearest active fault (m)	Distance from nearest fault (m)	Land use
1069	557.6	Crotone	Petilia Policastro	0	*D*	09.04.2013	09.04.2014	**1934.00**	86.00	*cS*	2404.7	1184.9	*Haa*
1103	577.0	Crotone	Verzino	0	*W*	09.04.2013	09.04.2014	1701.76	**165.59**	*fS*	7454.0	493.9	*Uf*
1101	574.2	Crotone	Verzino	0	*S*	09.04.2013	09.04.2014	1209.37	118.39	*fS*	**7492.6**	474.2	*Uf*
1100	548.1	Crotone	Verzino	0	*S*	09.04.2013	09.04.2014	1190.79	115.69	*fS*	7293.3	336.0	*Uf*
816	544.5	Catanzaro	Taverna	−1	*S*	11.02.2020	11.02.2021	1157.00	117.00	*aMa*	7467.7	38.5	*Uf*
568	207.1	Catanzaro	Lamezia Terme	−1	*W*	13.02.2014	13.02.2015	1144.82	36.31	*cS*	*360.2*	229.8	*Uf*
1044	540.6	Crotone	Pallagorio	0	*D*	18.03.2012	18.03.2013	1048.70	116.37	*cS*	5802.2	383.3	*Uf*
897	360.0	Crotone	Cirò	0	*S*	09.04.2013	09.04.2014	940.89	*18.27*	*cS*	6526.9	**3544.8**	*Haa*
1358	439.2	Vibo Valentia	San Costantino Calabro	0	*S*	16.10.2017	16.12.2018	*906.00*	92.00	*cS*	658.8	746.7	*Uf*

For each measurement, the following information is listed: ID (identifier); elevation a.s.l.; province; municipality; floor; type of building; start of measurement; end of measurement; concentration of activity; uncertainty; lithotype; distance from the nearest active/generic fault; land use (*lhaa: heterogeneous agricultural areas; uf. urban fabric*).

Table 5. Number of measurements by lithotype, taken inside (N^{in}) and outside (N^{out}) the buffers along the faults, for the whole sample.

Lithotype	N^{out}	N^{in}	N^{out} > 300 Bq m^{-3}	N^{in} > 300 Bq m^{-3}
cS	**908**	**51**	**63**	6
fS	88	12	10	1
LE	54	28	5	2
F	12	1	*0*	*0*
lM	44	4	4	2
mhM	77	12	8	1
aMa	104	37	9	**7**
bMa	*2*	*0*	1	*0*
Tot.	**1289**	**145**	**100**	**19**

For lithotypes, cf. text.

Table 6. Number of measurements (N), and range of concentrations by type of use of the building, for the ground floor subsample.

Type of use	N	Minimum (Bq m^{-3})	Maximum (Bq m^{-3})	N > 300 Bq m^{-3}
Dwelling	**399**	*6.77*	**1934.00**	**34**
School	363	**13.42**	*1209.36*	32
Workplace	*261*	12.00	1701.75	*16*
Tot.	**1023**			**82**

Table 7. Number of measurements by lithotype, taken inside (N^{in}) and outside (N^{out}) the buffers along the faults, for the ground floor subsample.

Lithotype	N^{out}	N^{in}	N^{out} > 300 Bq m^{-3}	N^{in} > 300 Bq m^{-3}
cS	**656**	**41**	**45**	4
fS	70	10	9	1
LE	40	18	2	1
F	9	1	*0*	*0*
lM	32	4	2	2
mhM	52	6	6	*0*
aMa	63	20	5	**5**
bMa	*1*	*0*	*0*	*0*
Tot.	**923**	**100**	**69**	**13**

For lithotypes, cf. text.

lithotypes (either inside or outside the fault buffers). In fact, 95% intervals of confidence largely overlap.

The variogram map of the Gaussian indoor radon data for the *sector of interest* did not show any relevant anisotropy. An isotropic experimental variogram was computed, and then modelled by using two basic structures: a nugget effect and an exponential model (Webster & Oliver, 2007) with a practical range of about 8700 meters. Since the exponential model has no finite range, a practical range equal to the distance at which the variogram equals 95% of the sill variance was used. The model shows a weak structure for the spatial distribution of indoor radon measurements, due to a short practical range compared to the extension of the *sector*, and the contribution of the nugget effect (about 37%) to the total sill. However, this spatial structure is not negligible and legitimated using a geostatistical approach for studying the indoor spatial distribution. The fitted model was then used with indoor radon data to generate 500 simulations by the *turning bands method*. A map of mean indoor concentration was obtained by averaging the 500 realizations (Figure E, scale 1:1,000,000). In such map, the spatial variation of radon is emphasized, without the typical smoothing effects of kriging.

For the same *sector*, the standard deviation of the 500 simulated concentrations, and the probability of exceeding the threshold of 300 Bq m^{-3} are shown in Figure 4(a,b, resp.). The highest values of uncertainty and of probability of exceedance are mainly to be found along the eastern border of the Sila massif (in the NE portion of the *sector*); subordinately, in the

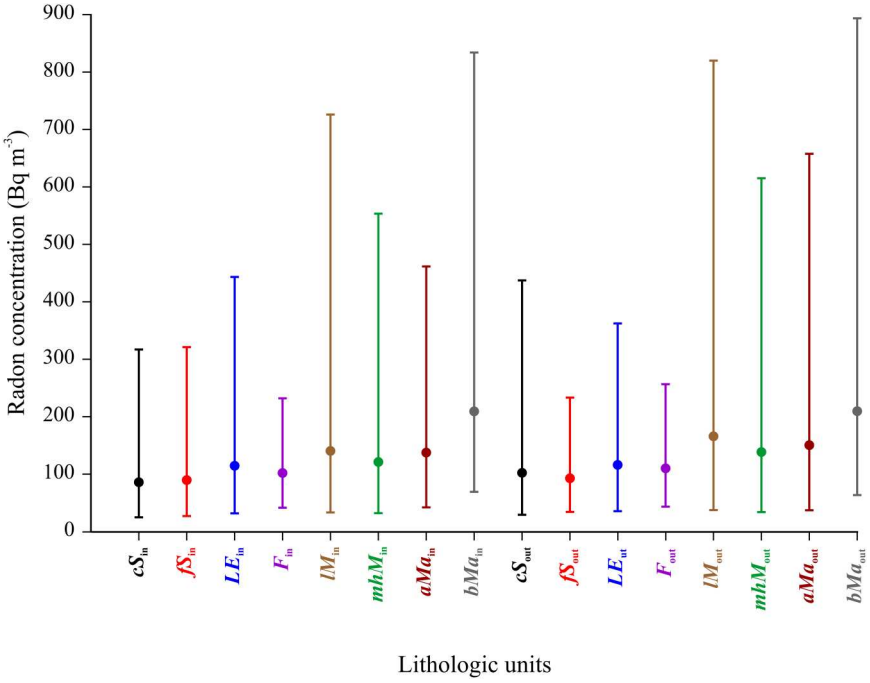

Figure 3. Mean values and their intervals of confidence (upper and lower limits at the 95% of confidence level) of indoor radon concentrations for the eight classes of lithotypes, inside or outside the fault buffers (subsample: ground floor). For lithotypes, see text. Subscripts '*in*' and '*out*' indicate locations '*within*' and '*outside*' the fault buffers, respectively.

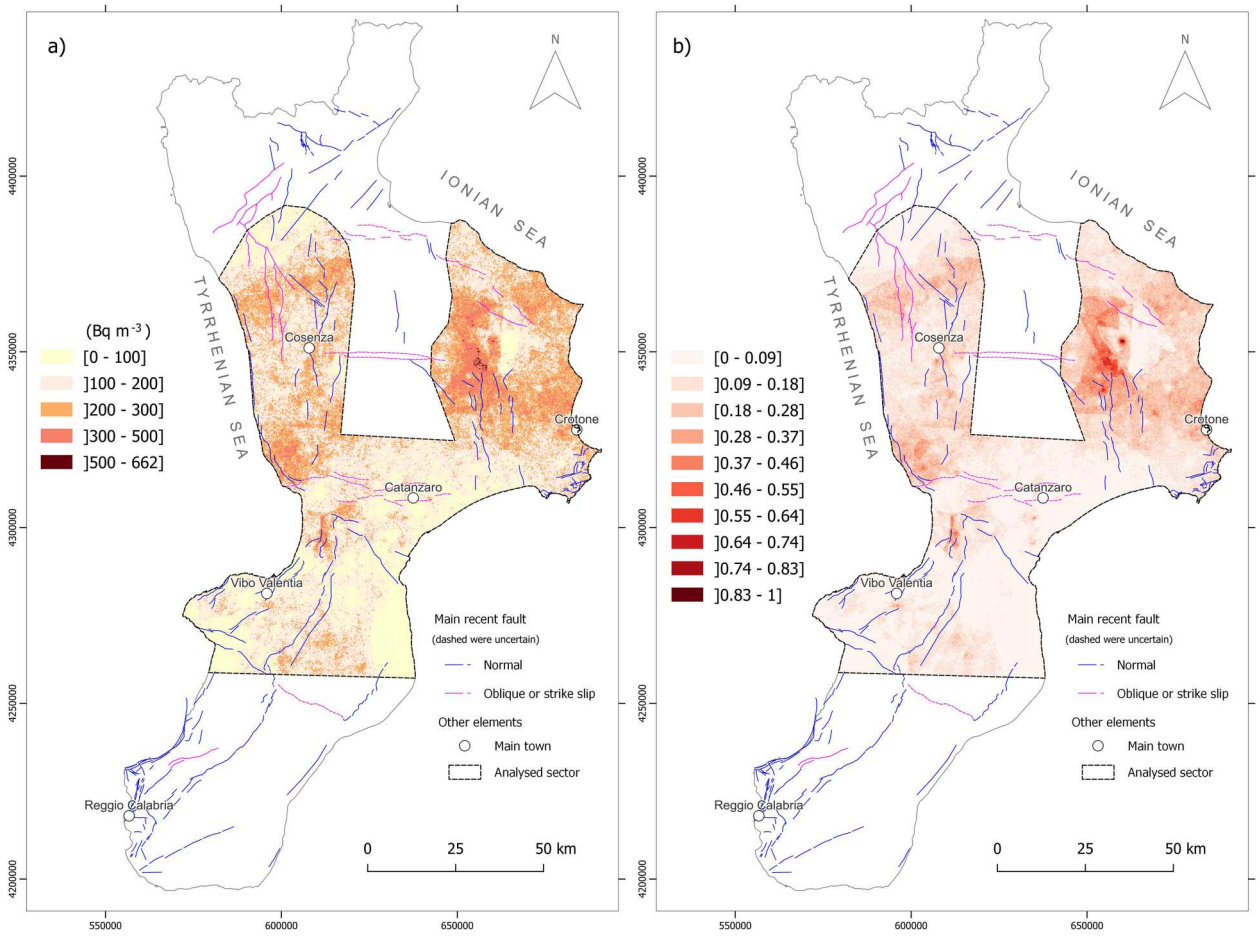

Figure 4. Post-elaboration maps of the realizations obtained by turning bands stochastic simulations for the *sector of interest*: (a) standard deviation of indoor radon concentration; (b) exceedance probability of the threshold (300 Bq m^{-3}).

western portion of the Lametia plain, and by the Tyrrhenian coast; quite high values also characterize the northern part of the Crati Graben. However, only 0.4% of the locations show probabilities greater than 50%.

In brief, the available set of measurements of indoor radon gas concentrations pointed out the highest values along the eastern border of the Sila massif (Northern Calabria), marked by the N-S regional fault system. Values above 900 Bq m^{-3} were mostly found in urbanized areas of the Crotone province, at ground floor of school buildings. From a geological point of view, such sites are located on coarse-grained sediments and not far from fault structures.

Overall, Figures 3, 4 and E help in delineating zones where anomalous (high) indoor concentrations are expected.

5. Conclusions

The analyses performed on indoor measurements showed no strong differences among lithotypes nor in relation to fault buffers. Indeed, mean concentrations, as well as their lower and upper limits, largely overlap, with intervals of confidence generally wider outside the fault buffers. Accordingly, a significant uncertainty characterizes mean values, and a greater number of measurement sites would be needed to explore these aspects in more detail. Nevertheless, the mentioned lack of strong control may, partly, be also explained by inadequate construction methods, and by the habits of people which may affect room ventilation.

As concerns the *sector of interest*, highest values of expected concentrations, as well as the greatest uncertainties and exceedance probabilities, are again located along the eastern border of the Sila massif. Therefore, such zones would also require additional measurements.

However, an appropriate optimisation approach for selecting new measurement points is strongly recommended, by properly considering geological constraints. Based on the preliminary results described in the present study, hopefully extended to further areas of Calabria, it may be possible to support urban planning policies and draw up recommendations to ensure proper constructive measures to counteract entry and accumulation of radon gas in the buildings.

Software

Statistical and geostatistical analyses were carried out by using Isatis® 2018.4 (www.geovariances.com). The

maps were realized by using the open sources software QGIS 3.20.

Geolocation information

Calabria, southern Italy.

Disclosure statement

No potential conflict of interest was reported by the author(s).

Data availability statement (DAS)

- The digital elevation model, derived from TINITALY (Tarquini et al., 2007), is available at http://tinitaly.pi.ingv.it/Download_Area2.html
- The main active and capable faults, derived from the ITHACA Catalogue (ITHACA, 2021), are available at http://sgi2.isprambiente.it/ithacaweb/viewer/
- Geological structures, derived from the Geological Map of Calabria (CASMEZ, 1969), are available at http://geoportale.regione.calabria.it/opendata
- Land use, derived from the Corine land cover 2012 – level 2, is available at https://land.copernicus.eu/pan-european/corine-land-cover/clc-2012?tab = download
- Indoor radon measurements are listed in Annex B. Due to privacy restrictions, the locations of the sites of measurement can only be shown at the Municipality level.

ORCID

Valeria Lupiano http://orcid.org/0000-0003-4255-0089
Gabriele Buttafuoco http://orcid.org/0000-0002-0280-8658
Valeria Rago http://orcid.org/0000-0001-7381-2227
Giulio Iovine http://orcid.org/0000-0002-8023-2973

References

Amodio-Morelli, L., Bonardi, G., Colonna, V., Dietrich, D., Giunta, G., Ippolito, F., Liguori, V., Lorenzoni, S., Paglionico, A., Perrone, V., Piccarreta, G., Russo, M., Scandone, P., Zanettin-Lorenzoni, E., & Zuppetta, A. (1976). L'Arco calabro-peloritano nell'orogene appennino-maghrebide. *Memorie Della Società Geologica Italiana*, *17*, 1–60.

Armstrong, M. (1998). *Basic linear geostatistics*. Springer Berlin Heidelberg. https://doi.org/10.1007/978-3-642-58727-6

Bing, S. (1993). CR-39 radon detector. *Nuclear Tracks and Radiation Measurements* 22, 451–454. https://doi.org/10.1016/0969-8078(93)90106-E

Buttafuoco, G., Tallarico, A., & Falcone, G. (2007). Mapping soil gas radon concentration: A comparative study of geostatistical methods. *Environmental Monitoring and Assessment*, *131*(1–3), 135–151. https://doi.org/10.1007/s10661-006-9463-7

Buttafuoco, G., Tallarico, A., Falcone, G., & Guagliardi, I. (2010). A geostatistical approach for mapping and uncertainty assessment of geogenic radon gas in soil in an area of southern Italy. *Environmental Earth Sciences*, *61*(3), 491–505. https://doi.org/10.1007/s12665-009-0360-6

Caers, J. (2011). *Modeling uncertainty in the earth sciences*. Chichester: John Wiley & Sons Ltd.

Cafaro, C., Bossew, P., Giovani, C., & Garavaglia, M. (2014). Definition of radon prone areas in Friuli Venezia Giulia region, Italy, using geostatistical tools. *Journal of Environmental Radioactivity*, *138*, 208–219. https://doi.org/10.1016/j.jenvrad.2014.09.003

CASMEZ. (1969). *Carta Geologica della Calabria in scala 1:25,000 (in Italian) [Geological map of Calabria at 1:25,000 scale]*.

Chilès, J.-P., & Delfiner, P. (2012). *Geostatistics: Modeling spatial uncertainty* (2nd ed.). John Wiley & Sons, Inc. https://doi.org/10.1002/9781118136188

Choubey, V. M., Bist, K. S., Saini, N. K., & Ramola, R. C. (1999). Relation between soil-gas radon variation and different lithotectonic units, Garhwal Himalaya, India. *Applied Radiation and Isotopes*, *51*(5), 587–592. https://doi.org/10.1016/S0969-8043(98)00149-3

Choubey, V. M., & Ramola, R. C. (1997). Correlation between geology and radon levels in groundwater, soil and indoor air in Bhilangana valley, Garhwal Himalaya, India. *Environmental Geology*, *32*(4), 258–262. https://doi.org/10.1007/s002540050215

Choubey, V. M., Sharma, K. K., & Ramola, R. C. (1997). Geology of radon occurrence around Jari in Parvati Valley, Himachal Pradesh, India. *Journal of Environmental Radioactivity*, *34*(2), 139–147. https://doi.org/10.1016/0265-931X(96)00024-0

Cinelli, G., Tollefsen, T., Bossew, P., Gruber, V., Bogucarskis, K., De Felice, L., & De Cort, M. (2019). Digital version of the European atlas of natural radiation. *Journal of Environmental Radioactivity*, *196*, 240–252. https://doi.org/10.1016/j.jenvrad.2018.02.008

Ciolini, R., & Mazed, D. (2010). Indoor radon concentration in geothermal areas of central Italy. *Journal of Environmental Radioactivity*, *101*(9), 712–716. https://doi.org/10.1016/j.jenvrad.2010.04.012

Clamp, G. E., & Pritchard, J. (1998). Investigation of fault position and sources of radon by measurement of 238U decay series radionuclide activity in soil samples. *Environmental Geochemistry and Health*, *20*(1), 39–44. https://doi.org/10.1023/A:1006525800379

Darby, S., Hill, D., Auvinen, A., Barros-Dios, J. M., Baysson, H., Bochicchio, F., Deo, H., Falk, R., Forastiere, F., Hakama, M., Heid, I., Kreienbrock, L., Kreuzer, M., Lagarde, F., Mäkeläinen, I., Muirhead, C., Oberaigner, W., Pershagen, G., Ruano-Ravina, A., … Doll, R. (2005). Radon in homes and risk of lung cancer: Collaborative analysis of individual data from 13 European case-control studies. *BMJ*, *330*(7485), 223. https://doi.org/10.1136/bmj.38308.477650.63

De Cort, M., Gruber, V., Tollefsen, T., Bossew, P., & Janssens, A. (2011). Towards a European atlas of natural radiation: Goal, status and future perspectives. *Radioprotection*, *46*(6), S737–S743. https://doi.org/10.1051/radiopro/20116871s

Fonseca, E. S. da. (1983). *Some characteristics of the CR-39 solid state nuclear - Track Detector for register of protons and low energy alpha particles*. Algumas caracteristicas

do detector solido de tracos CR-39 para registro de protons e particulas alfa de baixa energia.

Giustini, F., Ciotoli, G., Rinaldini, A., Ruggiero, L., & Voltaggio, M. (2019). Mapping the geogenic radon potential and radon risk by using empirical Bayesian Kriging regression: A case study from a volcanic area of central Italy. *Science of The Total Environment*, *661*, 449–464. https://doi.org/10.1016/j.scitotenv.2019.01.146

Goovaerts, P. (1997). *Geostatistical for natural resources evaluation*. New York: Oxford University Press.

Gundersen, L. C. S. (1992). The effect of rock type, grain size, sorting, permeability, and moisture on measurements of radon in soil gas: A comparison of two measurement techniques. *Journal of Radioanalytical and Nuclear Chemistry*, *161*(2), 325–337. https://doi.org/10.1007/BF02040479

Gundersen, L. C. S., Schumann, R. R., Otton, J. K., Dubiel, R. F., Owen, D. E., & Dickinson, K. A. (1992). Geology of radon in the United States. In *Geologic controls on radon*. Geological Society of America. https://doi.org/10.1130/SPE271-p1

Heuvelink, G. B. M. (2018). Uncertainty and uncertainty propagation in soil mapping and modelling. In A. B. McBratney, B. Minasny, & U. Stockmann (Eds.), *Pedometrics* (pp. 439–461). Springer International Publishing. https://doi.org/10.1007/978-3-319-63439-5_14

Ielsch, G., Thiéblemont, D., Labed, V., Richon, P., Tymen, G., Ferry, C., Robé, M. C., Baubron, J. C., & Béchennec, F. (2001). Radon (222Rn) level variations on a regional scale: Influence of the basement trace element (U, Th) geochemistry on radon exhalation rates. *Journal of Environmental Radioactivity*, *53*(1), 75–90. https://doi.org/10.1016/S0265-931X(00)00106-5

Iovine, G., Guagliardi, I., Bruno, C., Greco, R., Tallarico, A., Falcone, G., Lucà, F., & Buttafuoco, G. (2018). Soil-gas radon anomalies in three study areas of Central-Northern Calabria (Southern Italy). *Natural Hazards*, *91*(S1), 193–219. https://doi.org/10.1007/s11069-017-2839-x

ITHACA. (2021). *ITHACA Catalogue (ITaly HAzard from CApable faults)*. https://www.isprambiente.gov.it/it/progetti/cartella-progetti-in-corso/suolo-e-territorio-1/ithaca-catalogo-delle-faglie-capaci

Journel, A. G. (1983). Nonparametric estimation of spatial distributions. *Journal of the International Association for Mathematical Geology*, *15*, 445–468. https://doi.org/10.1007/BF01031292

Matheron, G. (1971). The theory of regionalized variables and its applications. In *Les Cahiers du Centre de Morphlogie Mathematique* (Vol. *5*, pp. 1–218). Ecole Nationale Superieure des Mines de Paris, Fontainebleau.

Matheron, G. (1973). The intrinsic random functions and their applications. *Advances in Applied Probability*, *5* (03), 439–468. https://doi.org/10.2307/1425829

Minda, M., Tóth, G., Horváth, I., Barnet, I., Hámori, K., & Tóth, E. (2009). Indoor radon mapping and its relation to geology in Hungary. *Environmental Geology*, *57*(3), 601–609. https://doi.org/10.1007/s00254-008-1329-6

Monaco, C., & Tortorici, L. (2000). Active faulting in the Calabrian arc and eastern Sicily. *Journal of Geodynamics*, *29*(3), 407–424. https://doi.org/10.1016/S0264-3707(99)00052-6

Nazaroff, W. W. (1992). Radon transport from soil to air. *Reviews of Geophysics*, *30*(2), 137–160. https://doi.org/10.1029/92RG00055

Sabbarese, C., Ambrosino, F., D'Onofrio, A., Pugliese, M., la Verde, G., D'Avino, V., & Roca, V. (2021). The first radon potential map of the Campania region (southern Italy). *Applied Geochemistry*, *126*, 104890. https://doi.org/10.1016/j.apgeochem.2021.104890

Steinbuch, M., Weinberg, C. R., Buckley, J. D., Robison, L. L., & Sandler, D. P. (1999). Indoor residential radon exposure and risk of childhood acute myeloid leukaemia. *British Journal of Cancer*, *81*(5), 900–906. https://doi.org/10.1038/sj.bjc.6690784

Tanner, A. B. (1964). Radon migration in the ground. In J. A. S. Adams & W. M. Lowder (Eds.), *The natural radiation environment* (pp. 161–190). University of Chicago Press. https://www.osti.gov/biblio/4500053

Tansi, C., Muto, F., Critelli, S., & Iovine, G. (2007). Neogene-Quaternary strike-slip tectonics in the central Calabrian Arc (southern Italy). *Journal of Geodynamics*, *43*(3), 393–414. https://doi.org/10.1016/j.jog.2006.10.006

Tansi, C., Tallarico, A., Iovine, G., Folino Gallo, M., & Falcone, G. (2005). Interpretation of radon anomalies in seismotectonic and tectonic-gravitational settings: The south-eastern Crati graben (Northern Calabria. *Italy)*. *Tectonophysics*, *396*(3–4), 181–193. https://doi.org/10.1016/j.tecto.2004.11.008

Tarquini, S., Isola, I., Favalli, M., & Battistini, A. (2007). *TINITALY, a digital elevation model of Italy with a 10 meters cell size (Version 1.0) [Data set]*. https://doi.org/10.13127/TINITALY/1.0

Tortorici, L., Monaco, C., Tansi, C., & Cocina, O. (1995). Recent and active tectonics in the Calabrian arc (southern Italy). *Tectonophysics*, *243*(1), 37–55. https://doi.org/10.1016/0040-1951(94)00190-K

Van Dijk, J. P., Bello, M., Brancaleoni, G. P., Cantarella, G., Costa, V., Frixa, A., Golfetto, F., Merlini, S., Riva, M., Torricelli, S., Toscano, C., & Zerilli, A. (2000). A regional structural model for the northern sector of the Calabrian Arc (southern Italy). *Tectonophysics*, *324*(4), 267–320. https://doi.org/10.1016/S0040-1951(00)00139-6

Vienneau, D., Boz, S., Forlin, L., Flückiger, B., de Hoogh, K., Berlin, C., Bochud, M., Bulliard, J. L., Zwahlen, M., & Röösli, M. (2021). Residential radon – comparative analysis of exposure models in Switzerland. *Environmental Pollution*, *271*, 116356. https://doi.org/10.1016/j.envpol.2020.116356

Wackernagel, H. (2003). *Multivariate geostatistics: An introduction with applications*. Springer.

Webster, R., & Oliver, M. A. (2007). *Geostatistics for environmental scientists*. John Wiley & Sons. Ltd. https://doi.org/10.1002/9780470517277

Zeeb, H., Shannoun, F., & Organization, W. H. (2009). *WHO handbook on indoor radon: A public health perspective*. World Health Organization.

Appendices

In Annex A, the villages considered in the survey are listed by province, with main statistics (n. of measurements, minimum, average, maximum and standard deviations) on the performed measurements.

In Annex B, the total set of measurement is listed. For each measurement, the following administrative and territorial features are shown: # (progressive number); ID (identifier); elevation a.s.l.; province; municipality; floor; type of building; start of measurement; end of measurement; concentration of activity; uncertainty; lithotype; distance from the nearest active fault; distance from the nearest generic fault; land use.